Songklanakarin J. Sci. Technol.
39 (6), 765-772, Nov. - Dec. 2017

http://www.sjst.psu.ac.th

Original Article

Mathematical model to predict heat transfer in transient condition of helical oscillating heat pipe

Narin Siriwan[1], Teerapat Chompookham[1], Yulong Ding[2], and Sampan Rittidech[1*]

[1] *Heat Pipe and Thermal Tools Design Research Unit (HTDR), Department of Mechanical Engineering, Faculty of Engineering, Mahasarakham University, Kantharawichai, Maha Sarakham, 44150 Thailand*

[2] *School of Chemical Engineering, University of Birmingham, Birmingham, United Kingdom*

Received: 21 January 2016; Revised: 5 September 2016; Accepted: 13 September 2016

Abstract

This research aims to study the heat transfer with a numerical model and experimental evaluation of a helical oscillating heat pipe (HOHP). Firstly, we created a numeric model of the HOHP to predict the time required to reach the steady state temperature and the heat transfer of the HOHP under transient conditions. Secondly, we measured the temperature at the pipe wall and evaluated the heat transfer rate from experiments and compared them with the numeric model. The results showed that the transient temperature and the heat transfer profiles of the HOHP from the numerical model were similar with the results measured from the experimental data. The results from numeric model predicted temperature profiles for attaining a steady state temperature were in close agreement, when compared to the numerical simulation of Boothaisong *et al*. (2015).

Keywords: mathematical model, heat transfer, transient, helical oscillating heat pipe

1. Introduction

The helical oscillating heat pipe (HOPH) is a type of heat pipe with a high heat transfer rate that is used for transferring heat from the heat source to the heat sink. The HOHP has a schematic is helical coil, therefore it will be used in heat transfer and application more than the conventional heat pipe, such as heat exchangers; and, helical coil heat exchangers are widely used in industrial applications, such as air refrigeration and conditioning (Akbaridoust *et al*., 2013).

In spite of their widespread use, there is little information available on the heat transfer in a helical coiled tube. Nobari and Malvandi (2013) studied the torsion and curvature effects on the fluid flow in a helical annulus. A second order finite difference method based on the projection algorithm was used to solve the governing equations in the helical coordinate system. They also considered the hydrodynamically fully developed flow and the effects of different physical parameters, such as curvature, torsion, pectratio, and Reynolds number, on the flow field. Saffari and Moosavi (2014) studied numerically the influence of the geometrical characteristics of a vertical helical coil on a bubbly flow. The turbulent single-phase and two-phase (air-water) bubbly fluid flows in a vertical helical coil were analyzed using computational fluid dynamics (CFD). They investigated the effects of the pipe diameter, coil diameter, coil pitch, Reynolds number, and void fraction on the pressure loss, friction coefficient, and flow characteristics. The three-dimensional equations governing the continuity, momentum, and energy were solved using the finite volume method. The k–ε turbulence model was used to calculate the turbulence fluctuations. The SIMPLE algorithm was employed to solve the velocity and pressure fields. Jayakumar *et al*. (2010) studied the CFD analysis of single-phase flows inside helically coiled tubes. They used CFD simulations to solve the governing equation of the helical coils by varying the coil parameters, such as the

* Corresponding author.
Email address: s.rittidech@hotmail.com

pitch circle diameter, the tube pitch, and the pipe diameter, and their influence on the heat transfer of the helical coil. Litster *et al*. (2006) studied the effect of curvature and torsion on the convective mass transfer in helical pipes, and they used 3D numerical analysis of the flow and mass transfer in helical pipes. The strong coupling between the torsion and curvature effects, and the resulting secondary flow regimes were well characterized by a parameter combining both the Dean and Germano numbers. Zhao *et al*. (2016) combined the high heat capacity of the PCM with the high thermal conductivity of the OHP can overcome the shortcomings of PCM itself, such as paraffin wax coupled with closed-loop oscillating heat pipe (CLOHP). They also designed the CLOHPs with different turns, manufactured and tested, and then a comprehensive investigation on the thermal performance of paraffin wax coupled with CLOHP under different supplied heating power was performed experimentally. Jiaqiang *et al*. (2016) studied a higher heat dissipation capacity of a closed oscillating heat pipe (COHP). In they work, a novel narrow-tube closed oscillating heat pipe model with two backward steps is proposed to enhance its heat transfer ability that is attributed to the oscillation cycle in a fixed direction. Volume of fluid (VOF) simulations and related experiments are performed to investigate the vapor, the temperature distribution and the thermal performance of the COHP. Jiaqiang *et al*. (2016) studied the distribution and fluctuation of pressure, vapor flow patterns, and the relationship between them during the starting process at different vacuum degrees of closed oscillating heat pipe. A two-dimensional model of the closed oscillating heat pipe was established, and the VOF (volume of fluid) model was taken as the solution to carry out the numerical simulation of liquid–vapor during the two-phase conversion.

There have been many studies related to the heat transfer of the helical coils, but they focused on steady state operation of the HOHP only. The HOHP also have operation at transient state operation, which it was very important thing in studies the heat transfer of the HOHP. Therefore, in this research aims to study the heat transfer with a numerical model and experimental evaluation of the HOHP. Firstly, we created a numeric model of the HOHP to predict the time required to reach the steady state temperature and the heat transfer of the HOHP under transient conditions. At last, we measured the temperature at the pipe wall and evaluated the heat transfer rate from experiments and compared them with the numeric model.

2. Mathematical Model

2.1 Geometry of helical oscillating heat pipe

A HOHP consists of three parts: the evaporator section (L_e), the adiabatic section (L_a) and the condenser section (L_c), as show in Figure 1 (Pipatpaiboon *et al*., 2012). Figure 2 shows the geometry of the HOHP with the coil radius r_a, the pitch p_s, the radius a (defined by the increase in elevation per revolution of coils $h_g = 2\pi p_s$), the curvature ratio κ and the torsion τ, which can be calculated using Equation 1 and 2,

$$\kappa = \frac{r_a^2}{(r_a^2 + p_s^2)} \tag{1}$$

$$\tau = \frac{p_s^2}{(r_a^2 + p_s^2)} \tag{2}$$

Figure 3 shows an orthogonal helical coordinate system. The basic governing equations for helical tubes can be represented in an orthogonal helical coordinate system, as suggested by Germano (1982). An orthogonal helical coordinate system can be introduced with respect to a master Cartesian coordinate system (x, y, z), by using the helical coordinates s for the axial direction, r for the radial direction and θ for the circumferential direction. The vector in the orthogonal coordinate system of a HOHP is $\vec{R}_{(s)}$, as calculated by Equation 3,

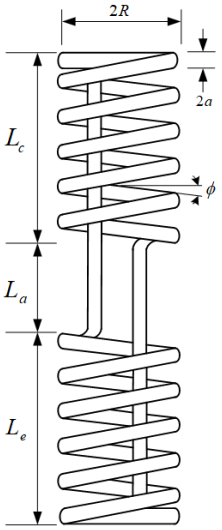

Figure 1. Schematic diagram of helical oscillating heat pipe (Pipatpaiboon *et al*., 2012).

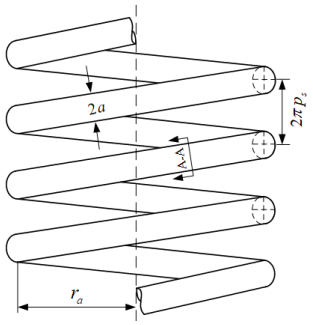

Figure 2. Geometry of helical oscillating heat pipe.

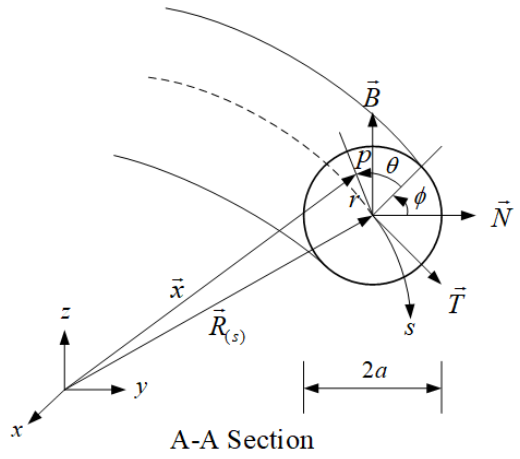

Figure 3. Orthogonal helical coordinate system (Germano, 1982).

$$\vec{R}_{(s)} = a\cos(s)\vec{i} + a\sin(s)\vec{j} + b(s)\vec{k} \quad (3)$$

The position of any given point p inside the helical pipe can be described by the vector $\vec{X}$, which can be calculated by Equation 4,

$$\vec{X} = \vec{R}_{(s)} - r\sin(\theta - \tau s)\vec{N}_{(s)} + r\cos(\theta - \tau s)\vec{B}_{(s)} \quad (4)$$

where $\vec{T}$, $\vec{N}$ and $\vec{B}$ are the tangential, normal and binormal directions to the generic curve of the pipe axis $\vec{R}_{(s)}$ at the point of consideration, respectively (Figure 3). The metric of the orthogonal helical coordinate system is given by Equation 5,

$$d\vec{x} \cdot d\vec{x} = (1 + \kappa r\sin(\theta - \tau s))^2 ds^2 + dr^2 + r^2 d\theta^2 \quad (5)$$

where dr, ds and $d\theta$ are the infinitesimal increments in the radial, axial and circumferential directions, respectively. With this metric, one obtains the scale factor h_s as given by equation (6),

$$h_s = 1 + \kappa r\sin(\theta - \tau s) \quad (6)$$

2.2 Governing equations

Governing equations for the calculated of the HOHP are the governing equation at the pipe wall and the vapor core. In addition, there is the governing equation for calculation of the heat transfer. All of which can be describe as in the following.

Pipe wall

The energy equation for the pipe wall used in the calculation for the pipe wall of the HOHP is given by Equation 7.

$$\rho_w c_{p,w} \frac{\partial T}{\partial t} = \frac{\partial}{\partial s}\left(k_w \frac{\partial T}{\partial s}\right) \quad (7)$$

where ρ_w is the density of the pipe wall, $c_{p,w}$ is the specific heat of the pipe wall and k_w is the thermal conductivity of the pipe wall.

Vapor core

The continuity, the momentum and the energy equations used in the calculation at the vapor core of the HOHP are given by Equations 8, 9, and 10, respectively (Akbaridoust *et al.*, 2013).

Continuity equation:

$$\frac{\partial rw}{\partial s} = 0 \quad (8)$$

Momentum equation:

$$\frac{\partial w}{\partial t} + \frac{1}{h_s}\left(\frac{\partial w}{\partial s}\right) + \frac{\kappa\sin(\theta - \tau s)}{h_s} w + \frac{\kappa\cos(\theta - \tau s)}{h_s} w = -\frac{1}{h_s}\frac{\partial p}{\partial s} + \frac{1}{\mathrm{Re}}\left[\frac{1}{h_s}\frac{\partial}{\partial s}\left(\frac{1}{rh_s}\frac{\partial rw}{\partial s}\right)\right] \quad (9)$$

Energy equation:

$$\frac{\partial T}{\partial t} + \frac{w}{h_s}\frac{\partial T}{\partial s} = \frac{1}{\mathrm{Re}\,\mathrm{Pr}\,h_s r}\frac{\partial}{\partial s}\left(\frac{r}{h_s}\frac{\partial T}{\partial s}\right) \quad (10)$$

Heat transfer

The heat transfer in the HOHP in this study has two parts: the numerical model and experiments. The numerical model was evaluated by calculating the temperatures at the pipe wall and the temperatures at the vapor core, which can be calculated by Equation 11 (Sakulchangsatjatai *et al.*, 2011). For the experiments, this was evaluated by taking measurements of the temperatures of the water at the inlet and outlet of the condenser section, which can be calculated by Equation 12 (Sriudom *et al.*, 2015).

Model:

$$Q_{out}^{new} = \pi D_i h(T_{v,i} - T_{w,i}) \quad (11)$$

where D_i is the inner diameter, h is the convection heat transfer coefficient at the condenser section, $T_{v,i}$ is the temperature of the vapor and $T_{w,i}$ is the temperature at the pipe wall.

Experimental:

$$Q = \dot{m}c_p(T_{out} - T_{in}) \quad (12)$$

where $\dot{m}$ is the mass flow rate, $c_{p,w}$ is the specific heat, T_{out} is the outlet temperature at the condenser section and T_{in} is the inlet temperature at the condenser section.

2.3 Initial and boundary conditions

The calculation needs to have the initial and the boundary conditions, which are the initial and the boundary conditions at the pipe wall and at the vapor core. The initial condition at the pipe wall and the vapor core for start-up of time ($t = 0$), are given as:

$$T = T_{w,ini} \quad \text{For the pipe wall}$$

$$T = T_{v,ini} \quad \text{For the vapor core}$$

where $T_{w,ini}$ is the initial condition of the pipe wall temperature and $T_{v,ini}$ is the initial condition of the vapor temperature. The boundary conditions at the pipe wall and the vapor core at the s coordinates have three different values for the outer wall and the vapor core: the evaporator, the adiabatic and the condenser sections. These are given as:

$$\left.\begin{aligned} T_{w,e} &= 60, 70, 80°C \\ T_{w,a} &= 25°C \\ T_{w,c} &= 20°C \end{aligned}\right\} \quad \text{For the pipe wall}$$

$$\left.\begin{aligned} T_{v,e} &= 60°C \\ T_{v,a} &= 25°C \\ T_{v,c} &= 20°C \end{aligned}\right\} \quad \text{For the vapor core}$$

where $T_{w,e}$, $T_{w,a}$ and $T_{w,c}$ are the initial temperatures conditions at the pipe walls of the evaporator, the adiabatic and the condenser sections, respectively. $T_{v,e}$, $T_{v,a}$ and $T_{v,c}$ are the initial temperatures conditions at the vapor core of the evaporator, the adiabatic and the condenser sections, respectively.

2.4 Numerical approach

The governing equations and boundary conditions were solved using the finite difference technique. The Crank-Nicolson method was utilized to solve the set of equations. The time step was taken according to the stability criteria, which depends on the grid size. In the present analysis, the time step was taken to be 10^{-9} sec. Grid independence was checked by examining the percentage change in the steady-state temperature at a fixed location. Results were obtained for 12 nodal points (along the direction).

The numerical procedure is showed in Figure 4. The calculation procedure of the simulation program was as follows: firstly, input the outer diameter (D_o), the inner diameter (D_i), the length of the evaporator (L_e), the adiabatic (L_a) and the condenser sections (L_c), the temperature of the evaporator (T_e) and the condenser sections (T_c) and working fluid within a HOHP. Secondly, start calculates at the first point $i = 1$. Thirdly, input the parameters at the pipe wall: the density (ρ_w), the specific heat ($C_{p,w}$), the thermal conductivity (k_w), the initial temperatures ($T_{w,ini}$) and the grid size in s direction (Δs). Next, the temperature at the pipe wall in the conduction equation was calculated. Fourthly, input the parameters at the vapor core for calculated in the continuity and momentum equations: the grid size in the s direction (Δs), the Reynolds number (Re), the scale factors (h_s), the pressure (p), the initial velocity (w_{ini}), the curvature ratio (κ), the inclination angle (θ) and the density (ρ). Next, calculate the velocity at the vapor in the continuity and momentum equations. Fifthly, input the parameters at the vapor core for calculated in the energy equation: the scale factors (h_s), the

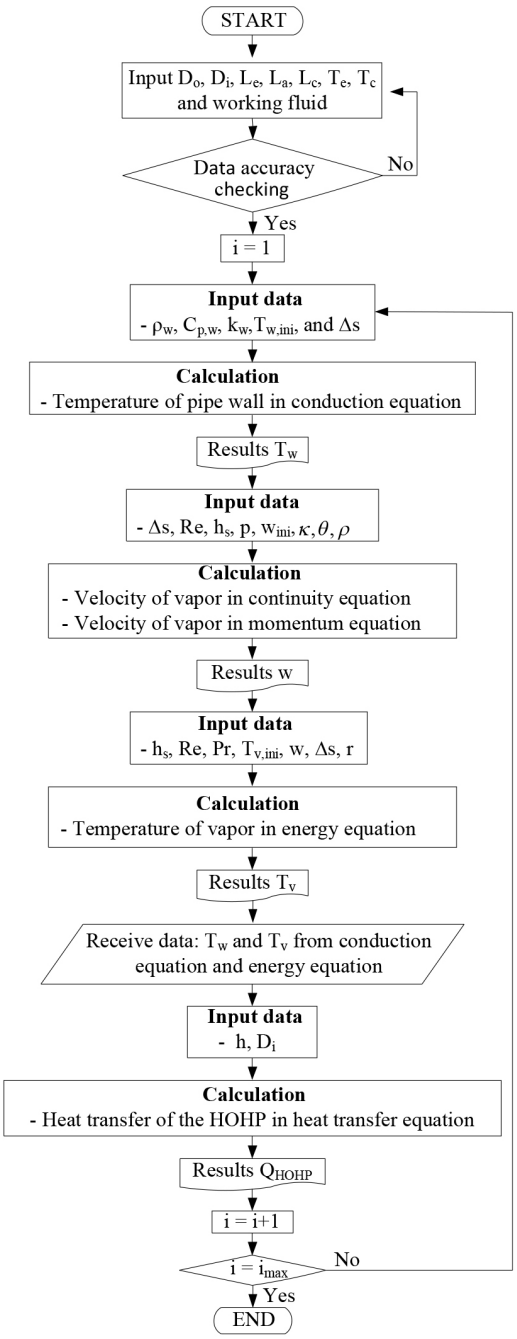

Figure 4. Flow chart for calculation heat transfer of helical oscillating heat pipe.

Reynolds number (Re), the Prandtl number (Pr), the initial temperature ($T_{v,ini}$), the velocity of the vapor (w), the grid size in the s direction (Δs) and the radial of the HOHP (r). Next, the temperature of the vapor in energy equation was calculated. Sixthly, receive data of the temperature: at the pipe wall (T_w) and at the vapor core (T_v) from the conduction and energy equation. Seventhly, input the parameters for calculated in heat transfer equation: the inner diameter (D_i) and the convection heat transfer coefficient (h). Next, calculate the heat transfer of the HOHP in the heat transfer equation. Eighthly, calculate at next point $i = i + 1$ and check the last point in the calculated, as whether this is equal to the maximum point or not. Ninthly, if the last point is equal to the maximum point, stop the calculation, or if not equal to the maximum point, return to calculation from start. When at the end of the calculation, the temperature should be changed from 60°C into 70°C and 80°C.

3. Experimental Setup

The HOHP used in this study was a copper pipe. R11 was used as the working fluid. The temperatures of the evaporator section were 60, 70 and 80°C. The temperature of the condenser section was 20°C. The mass flow rate was . The physical dimensions of the HOHP were defined as $L_e = 850$ mm, $L_a = 50$ mm, $L_c = 850$ mm, $D_o = 3.0$ mm and $D_i = 2.0$ mm. The physical properties at the pipe wall and the vapor core of the HOHP were open in table properties of the working fluid at the working temperatures (40, 45 and 50°C). The evaporator section of the HOHP was heated by a heat source and the condenser section was cooled by a heat sink, in which the heat source was hot water in an acrylic box and the heat sink was cool water in an acrylic box. The acrylic boxes were 120x120x120 mm (width x length x height) for both the evaporator and the condenser sections. Seventeen thermocouples were installed for data recording (Yokogawa DX200 with ±0.1°C accuracy, 20 channel input, and -200°C to 1100°C measurement temperature range). Type K thermocouples (OMEGA with ±0.1°C accuracy) were used to measure all of the temperatures at the specified times. The temperature measurement points were as follows: five points in the evaporator section, five points in the condenser section, two points in the adiabatic section, a point each in the inlet and outlet of the evaporator section, a point each in the inlet and outlet of the condenser section and a point in the ambient temperature. When determining the heat transfer from the experiments, the temperatures at the inlet and the outlet of the condenser section were used, and the calculation used Equation 12. The experimental setup with the test rig is shown in Figure 5 and a real experimental setup is shown in Figure 6.

4. Results and Discussion

The results of the temperatures at the pipe wall of the HOHP from the numeric model were compared with the experiments. For R11 as working fluid, the outer wall temperatures of the evaporator section were 60, 70 and 80°C are represented in Figures 7, 8 and 9 respectively. The transient temperature profiles were the average values for the evaporator, the adiabatic and the condenser sections and they were plotted as functions of time. It was found that the transient temperature profiles at the evaporator section increased from the initial temperature of the pipe wall to the outer temperatures at the evaporator section. In the adiabatic section, the transient temperature profiles increased to the working temperatures (the average temperature between the evaporator and the condenser sections). In the condenser section, the transient temperature profile decreased because the temperature of the outer wall was less than the initial temperature. The times required to reach the steady state temperature at the end of the runs from the numerical model for the evaporator section temperatures of 60, 70 and 80°C were about 1,100, 1,400 and 1,800 s, respectively. The times

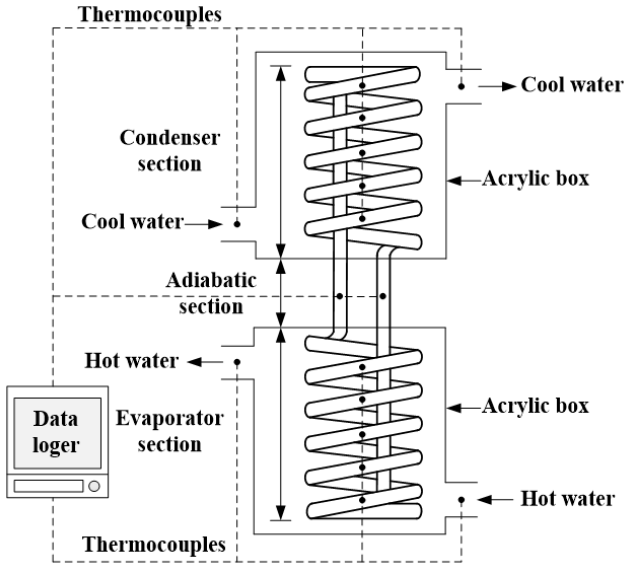

Figure 5. Schematic diagram in experimental setup of HOHP.

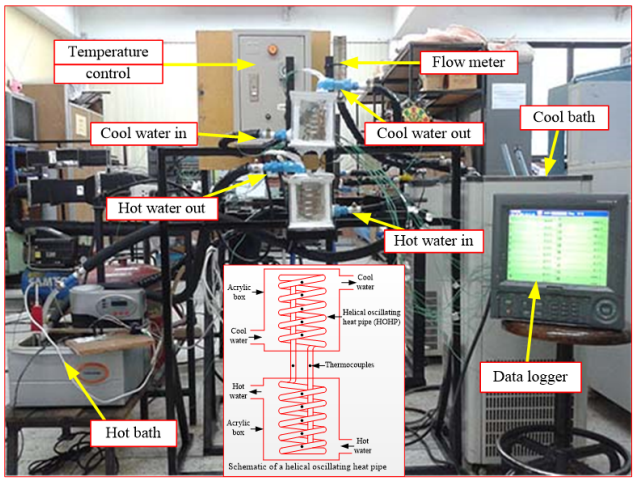

Figure 6. Experimental setup of HOHP.

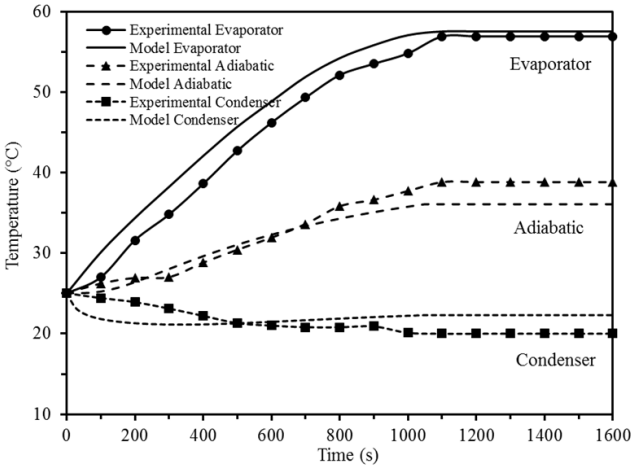

Figure 7. Comparison of temperature profiles at pipe wall of helical oscillating heat pipe between results from numeric model and experiments at T_e = 60°C for R11 as working fluid.

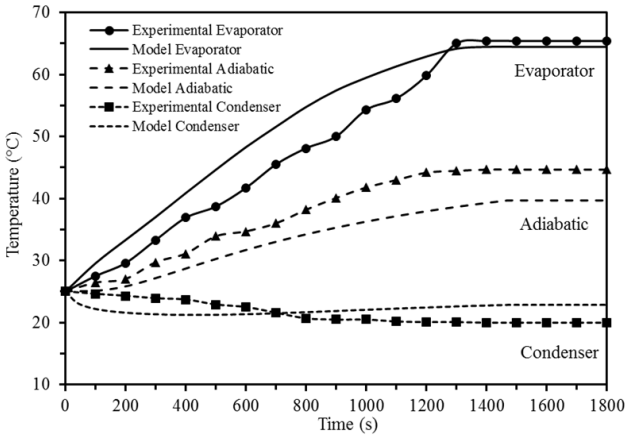

Figure 8. Comparison of temperature profiles at pipe wall of helical oscillating heat pipe between results from numeric model and experiments at T_e = 70°C for R11 as working fluid.

required to reach the steady state temperature from the experimental average values for the evaporator section temperatures of 60, 70 and 80°C were about 1,010, 1,380 and 1,618 s, respectively. It can be seen that, at the higher temperature of the evaporator section, the time to reach the steady state temperature was longer because the temperature was dependent on the time.

The solid lines correspond to the temperatures at the evaporator, the adiabatic and the condenser sections from the numerical model predicting the response of the temperature with time and the symbols correspond to the experimentally measured temperature average values. As can be seen form Figures 7, 8 and 9, the comparisons between the results of the numerical model and the experimental data response curves are excellent for all three sections. As seen from all the figures, the differences in the times required to reach the steady state temperatures between the numerical model and the experiment data for the evaporator section temperatures of 60, 70 and 80°C were about 8.2%, 1.4% and 10.1%, respectively. The time required to reach the steady state temperature is an important parameter for the start-up of the HOHP and the results from the numerical model and the experiment data were in good agreement.

Figure 10 shows the transient heat transfer profiles of the HOHP from the numeric model and the experiments for the evaporator section temperatures of 60, 70 and 80°C with R11 as working fluid. It was found that the times from start-up for the heat transfer from the numeric model and the experiments for the evaporator section temperature of 60°C were 400 and 396 s, for the evaporator section temperature of 70°C were 500 and 464 s and for the evaporator section temperature of 80°C were 600 and 520 s, respectively. Moreover, this figure shows the times required to reach the steady state heat transfer from the numeric model and the experiments for the evaporator section temperature of 60°C were 1,700 and

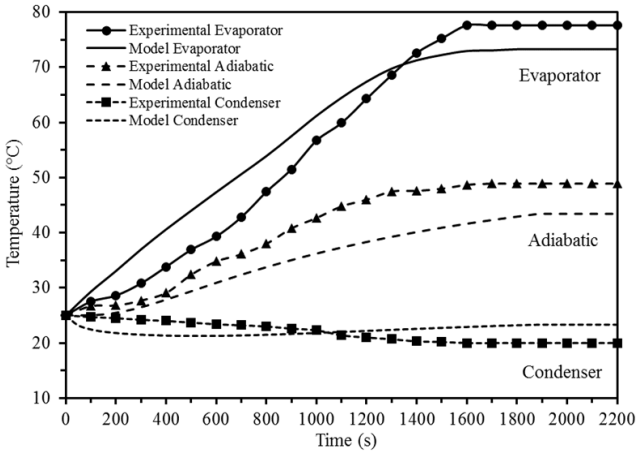

Figure 9. Comparison of temperature profiles at pipe wall of helical oscillating heat pipe between results from numeric model and experiments at T_e = 80°C for R11 as working fluid.

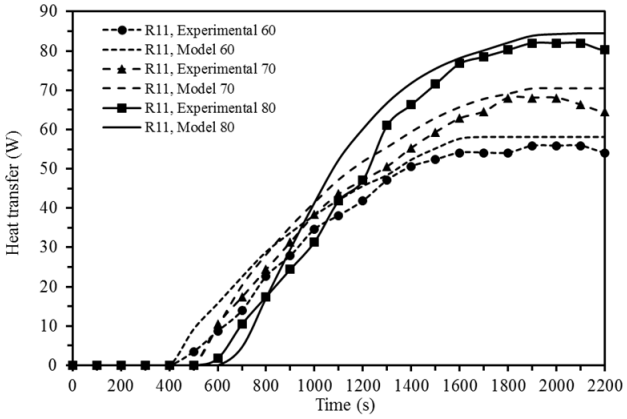

Figure 10. Comparison heat transfer of helical oscillating heat pipe from numeric model and experiments at T_e = 60, 70 and 80°C for R11 as working fluid.

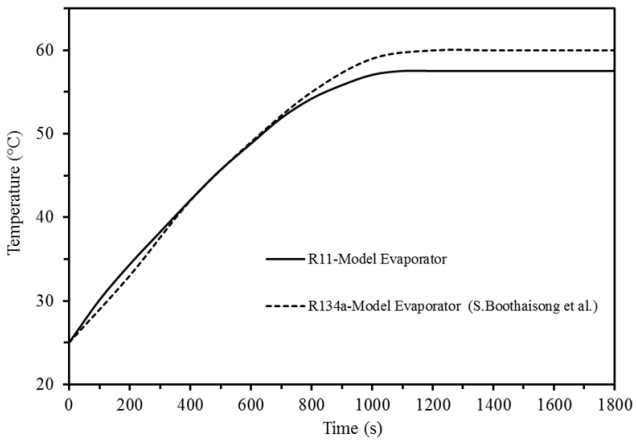

Figure 11. Comparison of temperatures profiles between this study and Boothaisong *et al*. (2015).

1,634 s, for the evaporator section temperature of 70°C were 1,900 and 1,818 s and for the evaporator section temperature of 80°C were 2,100 and 1,952 s. It can be seen that the time required to reach the steady state heat transfer depends on the temperature of evaporator section. The heat transfer profiles between the numeric model and the experiments were very similar, with the differences being 3.9%, 4.3% and 7.0% for the evaporator section temperatures of 60, 70 and 80°C, respectively.

Figure 11 shows a comparison of the temperature profile from this study and that obtained by Boothaisong *et al*. (2015). It was found that the temperature profiles of the heat pipe wall were in good agreement with the numeric model data in this study. The time required to reach the steady state temperature of the numeric model results from this study and the numeric model obtained by Boothaisong *et al*. (2015) were different due to differences in the heat input at the evaporator section, the working fluid used, the schematic and the parameters in analysis.

5. Conclusions

The temperature profiles from the numeric model, for both the transient and steady state, were successfully compared with the predictions from the experiments. The time required to reach the steady state temperature for the temperature of evaporator section of 60°C was about 16-18 min, for the temperature of evaporator section of 70°C was about 23-24 min, and for the temperature of evaporator section of 80°C was about 26-30 min. Moreover, the heat transfer profiles of the HOHP from the numerical model were successfully compared with the experiments. The time required for the steady state heat transfer for the temperature of evaporator section of 60°C was about 27-29 min, for the temperature of evaporator section of 70°C was about 30-32 min, and for the temperature of evaporator section of 80°C was about 32-35 min. In addition, the numeric model predicted temperature profiles for attaining a steady state temperature in this study were in close agreement, when compared to the numerical simulation of Boothaisong *et al*. (2015).

Acknowledgements

Authors gratefully acknowledge the Royal Golden Jubilee Ph.D. Program (Grant No. PHD/0014/2556) under the Thailand Research Fund (TRF) for funding this research.

References

Akbaridoust, F., Rakhsha, M., Abbassi, A., & Saffar-Avval, M. (2013). Experimental and numerical investigation of nanofluid heat transfer in helically coiled tubes at constant wall temperature using dispersion model. *International Journal of Heat and Mass Transfer*, *58*, 480-491.

Boothaisong, S., Ritidech, S., Chompookham, T., Thongmoon, M., Ding, Y., & Li, Y. (2015). Three-dimensional transient mathematical model to predict the heat transfer of a heat pipe. *Advances in Mechanical Engineering*, *7*(2), 1-11.

Germano, M. (1982). On the effect of torsion on a helical pipe flow. *Journal of Fluid Mechanics*, *125*, 1-8.

Jayakumar, J. S., Mahajani, S. M., Mandal, J. C., Iyer, K. N., & Vijayan, P. K. (2010). CFD analysis of single-phase flows inside helically coiled tubes. *Computers and Chemical Engineering, 34*, 430-446.

Jiateng, Z., Zhonghao, R., Chenzhen, L. & Yimin, L., (2016). Experiment al investigation on thermal performance of phase change material coupled with closed loop oscillating heat pipe (PCM/CLOHP) used in thermal management. *Applied Thermal Engineering, 93*, 90-100.

Jiaqiang, E., Xiaohuan, Z., Haili, L., Jianmei, C., Wei, Z., & Qingguo, P. (2016). Field synergy analysis for enhancing heat transfer capability of a novel narrow-tube closed oscillating heat pipe. *Applied Energy, 175*, 218-228.

Jiaqiang, E., Xiaohuan, Z., Yuanwang, D., & Hao, Z. (2016). Pressure distribution and flow characteristics of closed oscillating heat pipe during starting process at different vacuum degrees. *Applied Thermal Engineering, 93*, 166-173.

Litster, S., Pharoah, J. G., & Djilali, N. (2006). Convective mass transfer in helical pipes: effect of curvature and torsion. *Heat and Mass Transfer, 42*, 387-397.

Nobari, M. R. H., & Malvandi, A. (2013). Torsion and curvature effects on fluid flow in a helical annulus. *International Journal of Non-Linear Mechanics, 57*, 90-101.

Pipatpaiboon, N., Rittidech, S., Huchaiyaphum, H., Dangton, W., & Meena, P. (2012). Effect of Working Temperature on Heat Transfer Characteristic of Helix Oscillating Heat Pipe (HOHP). *International Conference Science*

4th. Technology and Innovation for Sustainable Well-Being (pp. 121-124). Pattaya, Thailand.

Saffari, H., & Moosavi, R. (2014). Numerical study of the influence of geometrical characteristics of a vertical helical coil on a bubbly flow. *Journal of Applied Mechanics and Technical Physics, 55*(6), 957-969.

Sakulchangsatjatai, P., Terdtoon, P., Wongratanaphisan, T., Kamonpet, P., & Murakami, M. (2004). Operation modeling of closed-end and closed-loop oscillating heat pipes at normal operating condition. *Applied Thermal Engineering. 24*, 995-1008.

Sriudom, Y., Rittidech, S., & Chompookham, T. (2015). The helical oscillating heat pipe: flow pattern behavior study. *Advances in Mechanical Engineering, 7*(1), 1-11.